Coronagraphic Low Order Wave Front Sensor : post-processing sensitivity enhancer for high performance coronagraphs

Frédéric P. A. Vogt[1], Frantz Martinache, Olivier Guyon, Takashi Yoshikawa, Kaito Yokochi, Vincent Garrel and Taro Matsuo

National Astronomical Observatory of Japan, Subaru Telescope, Hilo, HI 96720, USA

frantz@naoj.org

ABSTRACT

Detection and characterization of exoplanets by direct imaging requires a coronagraph designed to deliver high contrast at small angular separation. To achieve this, an accurate control of low order aberrations, such as pointing and focus errors, is essential to optimize coronagraphic rejection and avoid the possible confusion between exoplanet light and coronagraphic leaks in the science image. Simulations and laboratory prototyping have shown that a Coronagraphic Low Order Wave-Front Sensor (CLOWFS), using a single defocused image of a reflective focal plane ring, can be used to control tip-tilt to an accuracy of 10^{-3} λ/D. This paper demonstrates that the data acquired by CLOWFS can also be used in post-processing to calibrate residual coronagraphic leaks from the science image. Using both the CLOWFS camera and the science camera in the system, we quantify the accuracy of the method and its ability to successfully remove light due to low order errors from the science image. We also report the implementation and performance of the CLOWFS on the Subaru Coronagraphic Extreme AO (SCExAO) system and its expected on-sky performance. In the laboratory, with a level of disturbance similar to what is encountered in a post Adaptive Optics beam, CLOWFS post-processing has achieved speckle calibration to 1/300 of the raw speckle level. This is about 40 times better than could be done with an idealized PSF subtraction that does not rely on CLOWFS.

Subject headings: Extrasolar Planets — Astronomical Instrumentation

1. Introduction

Since the discovery of 51 Pegasi by Mayor & Queloz (1995), several hundreds extrasolar planets have been uncovered, for the most part via indirect detection methods such as radial velocity measurements of the reflex motion of their host star and photometric transit. Direct imaging was recently able to produce the first high contrast images of *solid* planetary candidates orbiting nearby main sequence stars: Fomalhaut (Kalas et al. 2008), Beta Pictoris (Lagrange et al. 2009) and HR 8799 (Marois et al. 2008; Lafrenière et al. 2009). Following up on these direct detections, Janson et al. (2010) obtained the first direct extrasolar planet spectrum, opening the way to better characterization of planetary atmospheres. These direct detections are currently limited to planets at large orbital separations of several dozens of AU, and only probe a small fraction of the distribution of known extrasolar planets, for which the median orbital separation is likely closer to 1 AU.

At near infrared wavelength, an 8-meter class telescope provides sufficient angular resolution (40 milli-arcseconds at λ=$\sim$1.6 μm) to be able to detect companions in the Habitable Zone of nearby stars (d $<$ 30 pc). High contrast imaging near the diffraction limit however requires very good control and calibration of the wavefront aberrations in the optical system. From the ground,

[1]Now at : Mount Stromlo and Siding Spring Observatories, Research School of Astronomy and Astrophysics, The Australian National University, Cotter Road, Weston Creek, ACT 2611, Australia.

this task is complicated by the rapidly changing atmospheric wavefront creating speckled images. While Adaptive Optics (AO) offers a major improvement, performance is still limited and direct imaging of planets often requires post-processing techniques such as Angular Differential Imaging (ADI) (Marois et al. 2006), which is most efficient at large ($\gtrapprox 10\ \lambda/D$) angular separations.

In the near future, high contrast imaging systems employing new coronagraphic and wavefront control techniques will greatly improve our ability to image exoplanets. These Extreme-AO systems include the Gemini Planet Imager (GPI) (Macintosh et al. 2006), ESO's SPHERE (Beuzit et al. 2008) and Subaru's SCExAO (Martinache & Guyon 2009). They will use efficient coronagraphs and high-speed high-order wavefront corrections to reduce speckles in the coronagraphic image. The images of the HR 8799 planetary system obtained by Serabyn et al. (2010) on a well-corrected 1.5 meter aperture using a high-performance coronagraph demonstrate the relevance of this approach.

Imaging companions close to the edge of the occulting mask in a coronagraph (that is ∼40 mas on SCExAO) however remains an unachieved feat. The current state of the art for PSF calibration is an optimized version of ADI called LOCI introduced by Lafrenière et al. (2007). LOCI can calibrate out high-order aberrations to a very high level of contrast (12 magnitudes and higher), but like any technique relying on ADI, only for angular separations greater than 10 λ/D. Detection at the edge of a $\sim 1\ \lambda/D$ occulter is extremely sensitive to low-order aberrations such as pointing and focus.

Of these aberrations, pointing is especially critical, since near the occulter, a tip-tilt excursion along a given direction mimics the signal of a true companion in a coronagraphic image. This issue, first identified for high contrast space borne coronagraphs, has been addressed by Guyon et al. (2009), with the Coronagraphic Low-Order Wavefront Sensor (CLOWFS), a scheme using the light occulted by a modified focal plane mask as an accurate pointing tracker.

The idea of using the light otherwise lost in the coronagraphic focal plane for tracking is not a novelty. It was for instance successfully implemented on the LYOT project (Digby et al. 2006). The calibration unit of GPI also uses the light occulted by the focal plane mask to measure low order aberrations, after re-imaging the pupil in a Shack Hartmann type wavefront sensor (Wallace et al. 2010): pointing performance with this scheme reaches 2 mas for typical expected observing conditions.

Maximum sensitivity to pointing errors is reached when the light from opposite edges of the pupil is allowed to interfere, which naturally happens in the focal plane. In this respect, while robust to a wide range of errors, a Shack-Hartman doesn't appear optimal to measure pointing: because it splits the pupil into sub-pupils, this capability is lost, resulting in lesser performance than a focal-plane based wavefront sensing scheme (Guyon 2005).

The originality of the CLOWFS design resides in its dual-zone focal plane mask, designed to suppress a strong offset to the signal, carrying most of the power but no information, in a manner reminiscent of strioscopy. The suppression of this offset turns the otherwise imperceptible changes due to small pointing errors into a macroscopic change of the CLOWFS image. Using this scheme, Guyon et al. (2009) were able to stabilize tip-tilt at the level of $10^{-3}\lambda/D$ in a closed-loop system for $\lambda = 633$ nm, in a laboratory experiment. The current implementation of CLOWFS on SCExAO exhibits pointing residuals <0.2 mas, with a 50 Hz frame rate.

While this level of performance is quite remarkable, we demonstrate in this work that additional calibration can be achieved in post-processing, and lead to an improved subtraction of coronagraphic leaks due to low-order aberrations in a long exposure. Using the SCExAO system as a testbed, we experimentally demonstrate a 40 times improvement of the detection limit over a classical calibration procedure at angular separation of a few λ/D.

This paper is organized as follows : in Section 2, we introduce how to use CLOWFS for post processing of coronagraphic images. In Section 3, we describe the implementation of the concept on the SCExAO experiment of the Subaru telescope, and we present our results in Section 4. In Section 5, we summarise our results and discuss possible updates to the presented CLOWFS configuration.

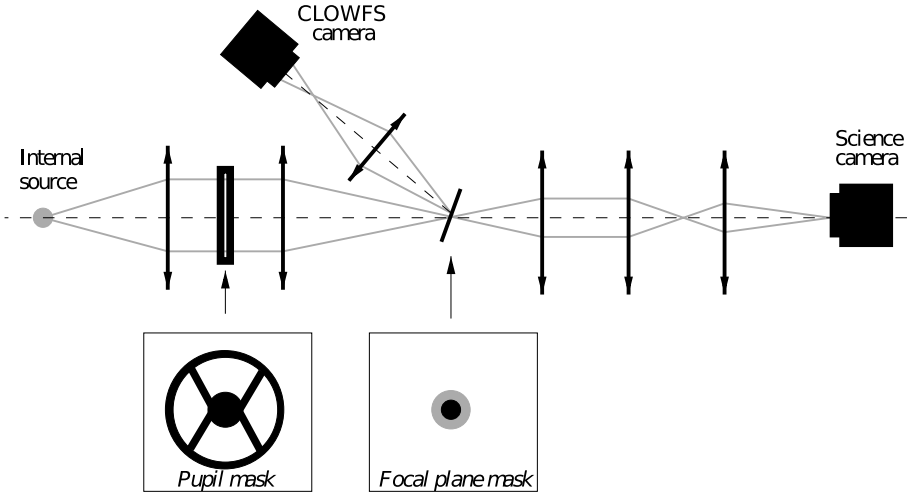

Fig. 1.— Optical layout of SCExAO used in Lyot-coronagraph mode. A mask lit by an IR ($\lambda = 1.55$ μm) laser diode emulates the Subaru Telescope pupil. The beam is focused on the dual-zone focal-plane occulting mask described in the text. The light reflected by the focal-plane mask feeds the (slightly defocused) CLOWFS detector, used to characterize pointing errors. The light that is not intercepted by the mask is then re-imaged on the "science" detector. Examples of images obtained on both cameras are presented in Fig. 2 and 4.

2. CLOWFS post-processing principle

A high performance PSF calibration procedure such as LOCI (Lafrenière et al. 2007), is based on a direct analysis of the science data alone. Yet near the edge of the coronagraphic mask, it is impossible, from such data only, to distinguish between the signal of an actual faint companion and the one of a systematic tip-tilt excursion off the coronagraphic mask at a given azimuth, that would be for instance due to a vibration. Data acquired with CLOWFS during a long exposure on the science camera can however be used to discriminate the two situations, in post-processing.

The scheme proposed in this paper is a form of adaptive optics PSF reconstruction, which uses measurements acquired in a wavefront sensor to estimate the long-exposure PSF in the science camera (Veran et al. 1997; Gendron et al. 2006). Adaptive Optics PSF reconstruction has been implemented on several adaptive optics systems (Harder & Chelli 2000; Jolissaint et al. 2010), and relies on the fact that the wavefront sensor, by measuring residual wavefront errors at a fixed spatial sampling, can be used to estimate the inner part of the PSF in the science camera. This estimation can be done at the wavefront sensing sampling speed (typically 100 Hz to 1kHz), and is then averaged for the duration of the science exposure. In this paper, we reconstruct the very inner part of the coronagraphic PSF using CLOWFS telemetry. Compared to previous implementations of adaptive optics PSF reconstruction, our scheme is better suited to high contrast coronagraphic imaging, as it uses a sensor which is highly sensitive to low order aberrations and free of non-common path errors. Our PSF reconstruction is however limited to the very inner part of the coronagraphic PSF, and is most effective in the 1 λ/D wide area immediately around the focal plane mask. At larger angular separation, wavefront errors can create speckles without producing a signal in the CLOWFS camera, and other calibration approaches must be used to reconstruct the PSF: for example telemetry from a higher order WFS, differential spectral imaging, or the ADI/LOCI technique. We also propose to use a new empirical image-based PSF reconstruction algorithm, where CLOWFS images are matched to science camera images to reconstruct the PSF, as opposed to relying on a model of the adaptive optics system. This empirical approach is more

robust, simple to implement, and is made possible in our case by the small number of modes measured by the CLOWFS.

A thorough description of the theory and hardware implementation of CLOWFS was provided by Guyon et al. (2009). Here, it suffices to remember that it operates thanks to an optimized dual zone focal plane mask, absorbing at its center, and reflective in an annulus whose outer edge defines the inner working angle of the system (1.5 λ/D for SCExAO). Figure 1 shows the actual implementation of CLOWFS on SCExAO. A lens re-images the reflective ring of the occulting mask on a detector deliberately placed out of focus, referred to as the CLOWFS camera.

During the (long) exposure on the science camera, the CLOWFS camera acquires a continuous stream of short (typically millisecond) exposures. An example of one such CLOWFS camera image is provided in Fig. 2: variations of the distribution of intensity in this image are used to identify drifts in pointing as well as changes in focus.

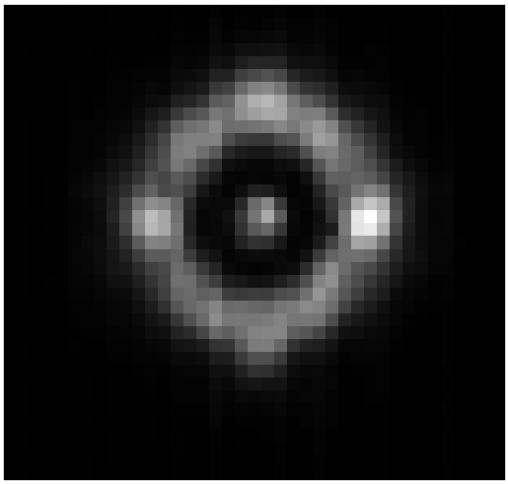

Fig. 2.— Example of CLOWFS camera image. Variations in the distribution of intensity in the image of the reflective annular region of the mask are used to track minute changes in the pointing.

Guyon et al. (2009) have demonstrated that over a small range ($\sim 0.2\lambda/D$) of pointing errors, a linear model relates the changes in CLOWFS images to the actual pointing error, and took advantage of this in a close-loop system, stabilizing the pointing at the level of $10^{-3}\lambda/D$ over extended periods of time ($\sim$ 1 hr).

Additional calibration of the coronagraphic leaks due to the residual tip-tilt error can be achieved in post-processing. This calibration relies on the one-to-one correspondence that exists between images simultaneously acquired on the science and the CLOWFS cameras. In either close or open loop, recording at high temporal rate CLOWFS images during a long exposure on the science camera can help predict the level of coronagraphic leaks attributable to pointing errors. A synthetic pointing leak image can be built and subtracted from the science image, to calibrate out the low-order aberrations residuals, ultimately improving contrast limits.

In its simplest version (see Section 5 for a discussion of the possible complements), the post-acquisition calibration of pointing errors with CLOWFS is a three-step procedure, described in the following sections and illustrated in Fig. 3.

- Step 1: calibrate the static optical configuration of the system (i.e. fine variations in optical path and alignment), using simultaneous pairs of images acquired with the science and the CLOWFS camera. This bank of pairs of images will be referred to as the dictionary (see Section 2.1).
- Step 2: track low-order modes during a long science exposure, continuously acquiring images at fast frame rate with the CLOWFS camera (see Section 2.2).
- Step 3: post processing of the data, by identifying a match for each CLOWFS image acquired during the science exposure in the dictionary (see Section 2.2).

2.1. System calibration: building up the dictionary

During step 1, pairs of simultaneous short exposure images are acquired with both the CLOWFS on a calibration source (internal source or single star). Images for exposure $\#k$ are respectively labeled DC_k and DS_k for the CLOWFS and science image. These images are stored into a database, called the dictionary.

After one such acquisition, as long as the optics remain stable, the CLOWFS image can be used as

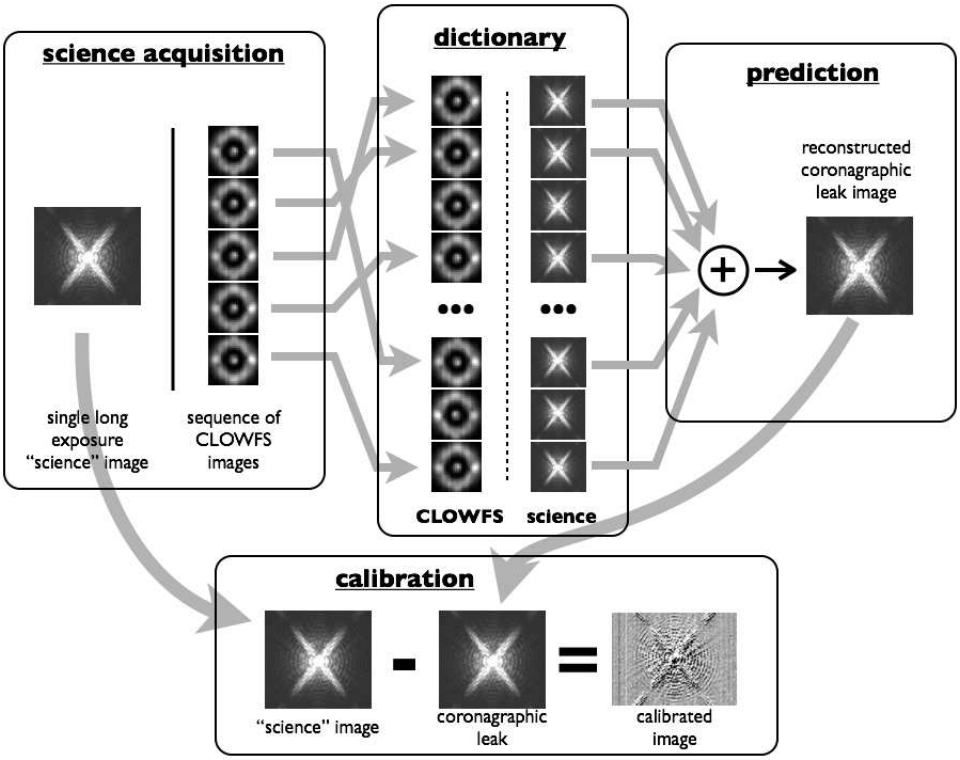

Fig. 3.— CLOWFS post-acquisition pointing errors calibration procedure, defined as the *Match-Maker* Algorithm (MMA).

a key that points to a coronagraphic leak term (the corresponding science image). Later, any instant CLOWFS image can be compared to the entries in the dictionary: the best matching entry in the dictionary allows to predict the amount of coronagraphic leak.

While slow varying non-common path errors can occur after the coronagraph, their effect can be kept small by minimizing the number of optics used after the CLOWFS focal-plane mask, as well as by regularly refreshing the content of the dictionary, so as to keep it up to date with the current status of the system.

A preliminary version of the dictionary can therefore be compiled in the lab prior to the actual observing, using a calibration source. However to minimize systematic error terms, it must be completed with more up-to-date images acquired on a series of calibration (non-resolved) stars of spectral type and magnitude comparable to the science target, so as to get the best possible match. Ideally, during acquisition on the calibration star, one wants to cover a range of pointing errors that is larger than experienced during the science exposure.

It is important to emphasize here that low-order aberrations errors are not explicitly calculated: instead, their consequences on the coronagraphic image are directly recorded, via the CLOWFS system. Pragmatic, this approach eliminates the need for a high fidelity (yet most likely imperfect) model of the coronagraph: ultimately, the ability to precisely characterize the coronagraphic leaks is determined by the coverage of the dictionary which can be made arbitrarily large.

2.2. Computing and subtracting coronagraphic leaks

During a long (i.e. typically greater than one second) exposure on the science camera, the CLOWFS camera acquires a sequence of short exposures (Step 2), labeled C_i that are saved along with the science camera image (cf. Fig. 3). To pre-

dict the coronagraphic leak in the science image, a matching algorithm (referred to as the *Match-Maker Algorithm*, or MMA) identifies each image of the CLOWFS sequence C_i to the CLOWFS image of the dictionary DC_k that best matches it. Fig. 2 shows the typical structure of one CLOWFS image. The region of interest within the image is defined as a disk circumscribing the ring visible in the image. The criterion used to evaluate the match is simply the pixel-to-pixel deviation between the two images, averaged over this region of interest:

$$\sigma(C_i, DC_k) = \sqrt{< (C_i - DC_k)^2 >} \qquad (1)$$

The operation is repeated for all images $(C_i)_{i=1}^{n}$ of the CLOWFS sequence. The matching short exposure science camera images (DS_k) of the dictionary are then co-added to form an estimate of the residuals in the long exposure coronagraphic image that can be attributed to varying low-order aberrations during the exposure on the science target. This final image is simply subtracted from the long exposure to calibrate these pointing error residuals.

3. Laboratory Demonstration

The experimental demonstration of the proposed post-processing technique was performed using the Subaru Coronagraphic Extreme-AO (SCExAO) bench in the Subaru laboratory (Martinache & Guyon 2009). Among extreme-AO systems, SCExAO specializes in the high-contrast characterization of the innermost (< 0.2 arc sec.) surrounding of stars, and in that scope, implements a high-performance PIAA-based (Guyon 2003) coronagraph that takes full benefit of the angular resolution of the 8-meter Subaru Telescope. For our test, the special optics described by Lozi et al. (2009) were taken out of the beam and SCExAO was reduced to a conventional near-IR Lyot-coronagraph without a Lyot-stop (see Aime & Soummer 2003, for an introduction to coronagraphy with apodized pupils). SCExAO is operated at IR wavelength (H-band), and uses two identical uncooled fast readout InGaAs cameras (Xenics model XS-1.7-320).

The light source is a $\lambda = 1.55\mu m$ laser diode, illuminating a 17-mm pupil mask emulating the Subaru Telescope pupil, producing the characteristic spikes in all the "science" images seen in this paper. The focal-plane mask is 85 μm in radius, which given the f-number of the beam gives a 4.75 λ/D inner working angle (IWA). Note that when the PIAA is inserted in the beam, the focal plane scale is altered (Guyon et al. 2005) and the IWA becomes $1.5\lambda/D$.

For this experiment, a 25 minute sequence of 15000 pairs of 1 millisecond exposure images were acquired with the CLOWFS and coronagraphic cameras on the SCExAO testbed at a $\sim$ 10 Hz frame rate. [1] A series of 150 contiguous pairs of images in the middle of this sequence were isolated to simulate a long-exposure acquisition. The science images were dark-subtracted and co-added to simulate a single long-exposure coronagraphic image. The corresponding sequence of raw CLOWFS images was simply stored (they form the $(C_i)_{i=0}^{149}$ list of images). The other 14850 pairs of images, labeled DC_k and DS_k were combined to form the dictionary.

The approach is illustrated by Fig. 4. The simulated Science frame (i.e. co-addition of the 150 selected images) is located in panel (a), while other panels compare the effect of two calibration procedures: standard PSF subtraction, as explained in Section 4.2 in panel (b) and the proposed CLOWFS post-processing procedure in panel (c).

4. Results

4.1. Best match for a CLOWFS image

For small wavefront aberrations, Guyon et al. (2009) showed that the CLOWFS image is a linear function of the low-order modes to be measured, typically (but not restricted to) pointing, focus and astigmatism. The approach proposed here only uses the average pixel-to-pixel deviation between two CLOWFS images, reducing the contribution of all these modes to a single scalar, and does not attempt at separating the different contributions.

To assess the extent of the coverage of these low-order modes by the dictionary, one can arbitrarily pick one image as reference, and calculate

[1] During recent engineering observations with SCExAO, the CLOWFS loop was successfully closed, using 5-10 ms exposures at an improved 50 Hz frame rate.

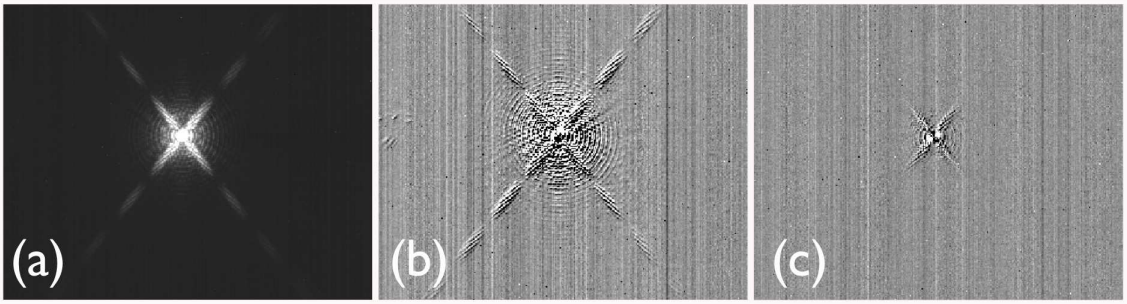

Fig. 4.— a) Long-exposure "science camera" image, non-linear intensity scale. Airy rings and diffraction spikes due to the peculiar Subaru Telescope pupil are clearly visible. b) Image after standard subtraction of a PSF without using the proposed CLOWFS image selection procedure. c) Image after CLOWFS post-processing calibration. Panels b and c use the same intensity scale.

the deviation of each image of the sequence, relative to this reference. Fig. 5 illustrates one such experiment, using image 5000 as reference. The value of this reduced CLOWFS signal ranges from σ ∼10: the level readout noise of the detector used for this experiment; to σ ∼140, with a mean at ∼55. Note for reference, that in this configuration, a pure pointing error of $0.4\lambda/D$ induces a reduced CLOWFS signal σ ∼110.

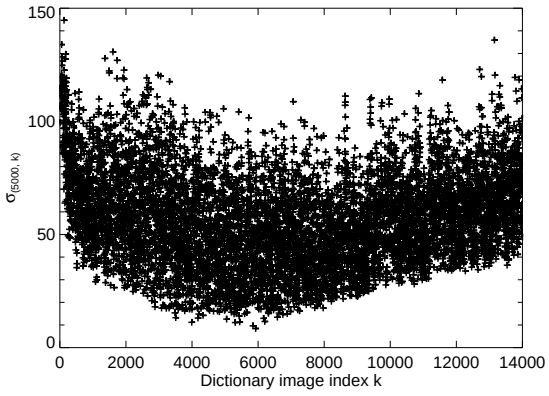

Fig. 5.— Evolution of the mean deviation $\sigma = \sqrt{< (DC_{5000} - DC_k)^2 >}$ over the 25-minute acquisition sequence of the dictionary, using image index 5000 as reference. In addition to the slow trend that moves the average signal measured over the course of the sequence, the effect of the source of vibration used on the bench is obvious as a most of the recorded range of signal is explored in less than a minute.

The 25-minute sequence of signal was acquired with a strong source of vibration (an electric water pump) bolted to the bench, next to the focal plane. In addition to the low trend visible on Fig. 5, the fast vibration makes that CLOWFS quickly explores the full range of aberrations covered during this experiment. While building the dictionary, it is important to cover a sufficiently wide amplitude of low-order modes signal, as in the post-processing step, it improves the odds for the matching algorithm to find a dictionary image that matches any CLOWFS image.

Fig. 6, shows as a solid line the value of the mean deviation σ between each image of the CLOWFS sequence its best dictionary match. Hardly differentiable from the solid line is a dotted line, showing the deviation with the 2^{nd} best match. For these two virtually identical cases, the deviation is dominated by the detector readout noise (∼10 ADU per pixel). A randomly chosen dictionary image (dash-dotted line) exhibits a mean deviation in average ten times as large.

4.2. Calibration of coronagraphic leaks

Fig. 4 illustrates the significant improvement that the calibration of low-order aberration induced coronagraphic leaks with CLOWFS offers (c) over a more standard PSF subtraction (b).

The standard PSF subtraction shown in (b) was derived from the data without knowledge of the CLOWFS frames. To simulate the standard acquisition of a PSF for calibration in a fair manner (in practice, this implies to find a single star of

comparable brightness and spectral type, located at a comparable elevation), we randomly selected a number of images corresponding to the total science exposure duration from the science side of the dictionary and co-added them to form a second long-exposure frame simulation. Fig. 4 (b) shows the residuals after the PSF subtraction. While the outer part of the image is dominated by detector readout, the scientifically valuable central part of the field is dominated by residual speckle noise.

To produce the calibrated PSF shown in (c), the science images corresponding to indices selected by the MMA procedure are co-added to form what should be a very good PSF for the calibration of a coronagraphic image. The residual speckle level in this calibrated PSF is much lower than for the standard PSF subtraction.

While only one example is provided in Fig. 4, a total of 200 different PSFs were also simulated, in order to provide a statistically relevant comparison between the CLOWFS and standard PSF subtraction residuals. Fig. 7 shows together all the radial profiles of raw, standard-PSF-subtracted and CLOWFS-PSF-subtracted images. Each of the 200 simulated PSFs offer an improvement of the contrast over the entire field of view by a factor ten, in comparison with the raw image. In comparison, the CLOWFS PSF improves the calibration by almost two orders of magnitudes between the inner working angle of the Lyot-coronagraph (4.75 λ/D) and $\sim 20\lambda/D$, where the contrast reaches the detector readout noise floor. In practice, a standard PSF subtraction would require a change of the pointing of the telescope to observe a calibration star. Such a change will change the structure of static aberrations, introducing a systematic error that will degrade actual performance of the PSF subtraction in comparison with what is presented here. On sky, CLOWFS-like calibrations are likely to prove even more advantageous.

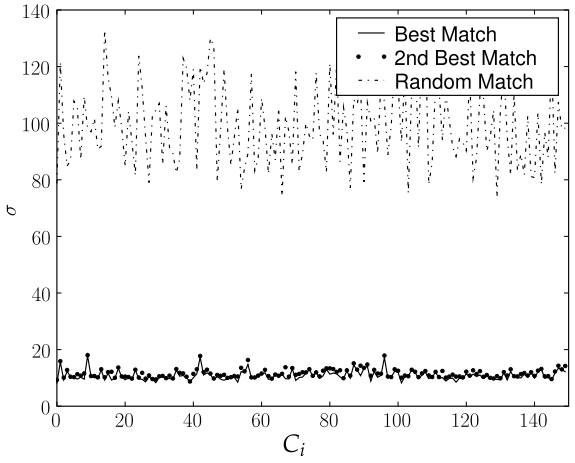

Fig. 6.— Mean deviation σ in between each image C_i of the CLOWFS sequence and its respective best and second best fit (full line and dots). The dash-dotted line shows the same deviation, this time between C_i and a random CLOWFS image, averaged over 200 experiments.

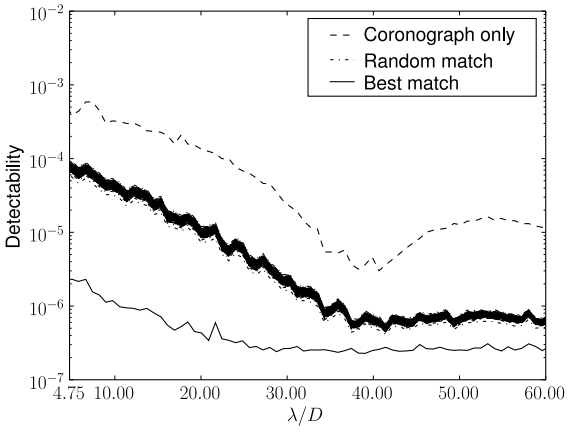

Fig. 7.— Standard deviation of the image profile as a function of angular separation. The figure compares three types of profiles: the raw science image (dashed line), the best-fit cleaned science image (solid line) using the proposed post-processing procedure and 200 random-match cleaned science images (dot-dashed line) simulating the standard PSF subtraction.

5. Conclusion

The results presented in Sec 4 demonstrate that, used in post-processing, CLOWFS improves the sensitivity of a coronagraph by a factor 40, in comparison to more conventional -yet idealized- type of calibration. The method described here for this proof of concept is yet still quite rudimentary, and could benefit from several improvements.

Instead of relying on an exhaustive search by

a MMA-like algorithm on a massive database, necessarily containing redundant information, the dictionary could be simplified using approaches like Principal Component Analysis, in which CLOWFS images would be projected onto a smaller sub-set of CLOWFS modes. In addition, an extended knowledge of several experimental parameters, such as the telescope elevation, star color or magnitude, could be implemented in the dictionary so as to improve on the actual calibration.

The approach is nevertheless powerful as it requires neither modelling of the coronagraph, nor assumptions such as linearity of the response in order to work. The absence of such requirements makes it extremely robust, and able to handle multiple situations and types of coronagraphic leaks.

The Subaru Coronagraphic Extreme AO Project implements a CLOWFS, used in close-loop. The system architecture however allows for a simple implementation of the CLOWFS post-processing, with no impact on the hardware, to calibrate residual low-order modes induced coronagraphic leaks. CLOWFS on SCExAO currently generates a steady 4 Mbits/s data stream. While not prohibitively large for an experiment, the storage of entire nights of CLOWFS data will quickly prove impractical as SCExAO enters a more aggressive observing phase. Eventually, the calibration of coronagraphic leaks using CLOWFS will require the matching to be performed on-the-fly, so that only the final coronagraphic leak image is actually saved.

Because it makes no assumption on targets and the current state of the optical bench, CLOWFS used both for live and post-processing is likely to play a significant part to the success of SCExAO, focused on the detection of planetary companions at small angular separation.

Frédéric Vogt thanks Brian Elms for sharing his experience and the machining of parts used for this project.

Facilities: Subaru (SCExAO).

REFERENCES

Aime, C. & Soummer, R. 2003, in EAS Publications Series, Vol. 8, EAS Publications Series, ed. C. Aime & R. Soummer, 79–92

Beuzit, J., Feldt, M., Dohlen, K., et al. 2008, in Society of Photo-Optical Instrumentation Engineers (SPIE) Conference Series, Vol. 7014, Society of Photo-Optical Instrumentation Engineers (SPIE) Conference Series

Digby, A. P., Hinkley, S., Oppenheimer, B. R., et al. 2006, ApJ, 650, 484

Gendron, E., Clénet, Y., Fusco, T., & Rousset, G. 2006, A&A, 457, 359

Guyon, O. 2003, A&A, 404, 379

Guyon, O. 2005, ApJ, 629, 592

Guyon, O., Matsuo, T., & Angel, R. 2009, ApJ, 693, 75

Guyon, O., Pluzhnik, E. A., Galicher, R., et al. 2005, ApJ, 622, 744

Harder, S. & Chelli, A. 2000, A&AS, 142, 119

Janson, M., Bergfors, C., Goto, M., Brandner, W., & Lafrenière, D. 2010, ApJL, 710, L35

Jolissaint, L., Christou, J., Wizinowich, P., & Tolstoy, E. 2010, in Society of Photo-Optical Instrumentation Engineers (SPIE) Conference Series, Vol. 7736, Society of Photo-Optical Instrumentation Engineers (SPIE) Conference Series

Kalas, P., Graham, J. R., Chiang, E., et al. 2008, Science, 322, 1345

Lafrenière, D., Marois, C., Doyon, R., & Barman, T. 2009, ApJL, 694, L148

Lafrenière, D., Marois, C., Doyon, R., Nadeau, D., & Artigau, É. 2007, ApJ, 660, 770

Lagrange, A., Gratadour, D., Chauvin, G., et al. 2009, A&A, 493, L21

Lozi, J., Martinache, F., & Guyon, O. 2009, PASP, 121, 1232

Macintosh, B., Graham, J., Palmer, D., et al. 2006, in Society of Photo-Optical Instrumentation Engineers (SPIE) Conference Series, Vol. 6272, Society of Photo-Optical Instrumentation Engineers (SPIE) Conference Series

Marois, C., Lafrenière, D., Doyon, R., Macintosh, B., & Nadeau, D. 2006, ApJ, 641, 556

Marois, C., Macintosh, B., Barman, T., et al. 2008, Science, 322, 1348

Martinache, F. & Guyon, O. 2009, in Society of Photo-Optical Instrumentation Engineers (SPIE) Conference Series, Vol. 7440, Society of Photo-Optical Instrumentation Engineers (SPIE) Conference Series

Mayor, M. & Queloz, D. 1995, Nature, 378, 355

Serabyn, G., Mawet, D., & Burruss, R. 2010, in Bulletin of the American Astronomical Society, Vol. 41, Bulletin of the American Astronomical Society, 587–+

Veran, J.-P., Rigaut, F., Maitre, H., & Rouan, D. 1997, Journal of the Optical Society of America A, 14, 3057

Wallace, J. K., Burruss, R. S., Bartos, R. D., et al. 2010, in Society of Photo-Optical Instrumentation Engineers (SPIE) Conference Series, Vol. 7736, Society of Photo-Optical Instrumentation Engineers (SPIE) Conference Series

This 2-column preprint was prepared with the AAS LaTeX macros v5.2.